ACS APPLIED MATERIALS & INTERFACES

RESEARCH ARTICLE

www.acsami.org

Sonochemical Synthesis of Ordered SnO_2/CMK-3 Nanocomposites and Their Lithium Storage Properties

Hui Qiao, Jing Li, Jiapeng Fu, Dnt Kumar, Qufu Wei,* Yibing Cai, and Fenglin Huang*

Key Laboratory of Eco-textiles, Ministry of Education, Jiangnan University, Wuxi 214122, P.R. China

ABSTRACT: In this study, we successfully prepare SnO_2 nanoparticles inside the pore channels of CMK-3 ordered mesoporous carbon via sonochemical method. The content of SnO_2 is 17 wt % calculated according to the energy-dispersive X-ray spectroscopy (EDS) result. CMK-3 with 17 wt % loading of SnO_2 nanoparticles has a large specific surface area and pore volume. Electrochemical performance demonstrates that the ordered SnO_2/CMK-3 nanocomposites electrode possesses higher reversible capacity and cycling stability than that of original CMK-3 electrode. Moreover, the ordered SnO_2/CMK-3 nanocomposites electrode also exhibits high capacity at higher charge/discharge rate. The improved electrochemical performance is attributed to the nanometer-sized SnO_2 formed inside CMK-3 and the large surface area of the mesopores (3.4 nm) in which the SnO_2 nanoparticles are formed.

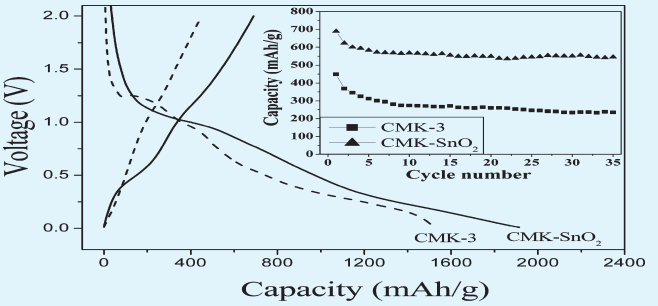

KEYWORDS: sonochemical method, ordered SnO_2/CMK-3, nanocomposites, anode, lithium-ion batteries

Carbonaceous material is a major material for the negative electrode in the rechargeable lithium battery because it exhibits both higher specific capacity, long cycle life, and no memory effect.[1−4] The carbonaceous material electrodes have several problems hinder practical application in rechargeable lithium batteries:[5−7] (1) a high irreversible specific capacity; (2) poor cycling performance; (3) too low an intercalating potential, which is closer to or exceeds 0 V.

Recently, much attention has been focused on the ordered mesoporous carbons (CMK-3) anode material, which is a silica-templated mesoporous carbon with uniform mesopores and a large surface area.[8−11] The ordered mesochannel and the large surface area of CMK-3 shorten the distance of Li-ion diffusing and its high conductivity is in favor of transmitting the electrons.[8] Zhou et al.[8] reported that the first discharge capacity of the ordered mesoporous carbon material was 3100 mAh·g^{-1}, which was eight times higher than the theoretical value of LiC_6. However, the initial Coulombic efficiency was only about 34%. The irreversible capacity was almost 2000 mA h g^{-1}, which is attributed to the formation of SEI films on the large surface area. Moreover, the material showed unsatisfactory capacity retention with cycling.

SnO_2 has attracted much attention, as it offers a promising alternative to carbon based anode materials in lithium-ion batteries. This is due to its large specific charge capacity.[12−17] However, the practical implementation of SnO_2 is hampered by its poor cycling stability arising from the large specific volume change (about 358%) in repetitive charging and discharging of the battery, which causes mechanical failure and loss of electrical contact at the anode.[18,19]

Sonochemical method was a useful technique for rapidly synthesizing novel materials with unusual properties.[20−24] The chemical effects of ultrasound were due to acoustic cavitation phenomena that cause the formation, growth, and collapse of bubbles in a liquid. The acoustic cavitations produce reactive radicals from water or other radical sources in aqueous solution. These reactive radicals with extremely high temperature, pressure, and cooling rates confer unique properties on sonicated solutions, and reduce metal ions to metal or metal oxide nanoparticles. Sonochemical methods have been employed successfully in preparing mesoporous metal oxides[25,26] and mesoporous composites.[27−29]

In this study, we prepared SnO_2 nanoparticles inside the pore channels of ordered mesoporous carbon CMK-3 (ordered SnO_2/CMK-3 nanocomposites) via sonochemical method. Electrochemical performance demonstrated that the ordered SnO_2/CMK-3 nanocomposites electrode exhibited a large initial discharge capacity of 690 mA h g^{-1} and excellent cycling performance, the reversible capacity of 546 mA h g^{-1} was retained after 35 cycles, much higher than that of original CMK-3 electrode (234 mA h g^{-1}). Furthermore, the ordered SnO_2/CMK-3 nanocomposites electrode also exhibited high capacity at higher charge/discharge rate, suggesting its excellent rate capability.

The diffraction peaks of [100], [110], and [200] in the hexagonal structure can be observed in the small-angle X-ray diffraction (XRD) pattern shown in Figure 1a, which can be indexed to the typical of ordered mesoporous carbon. The three peaks were detected both in ordered SnO_2/CMK-3 nanocomposites in the

Received: July 6, 2011
Accepted: August 23, 2011
Published: August 23, 2011

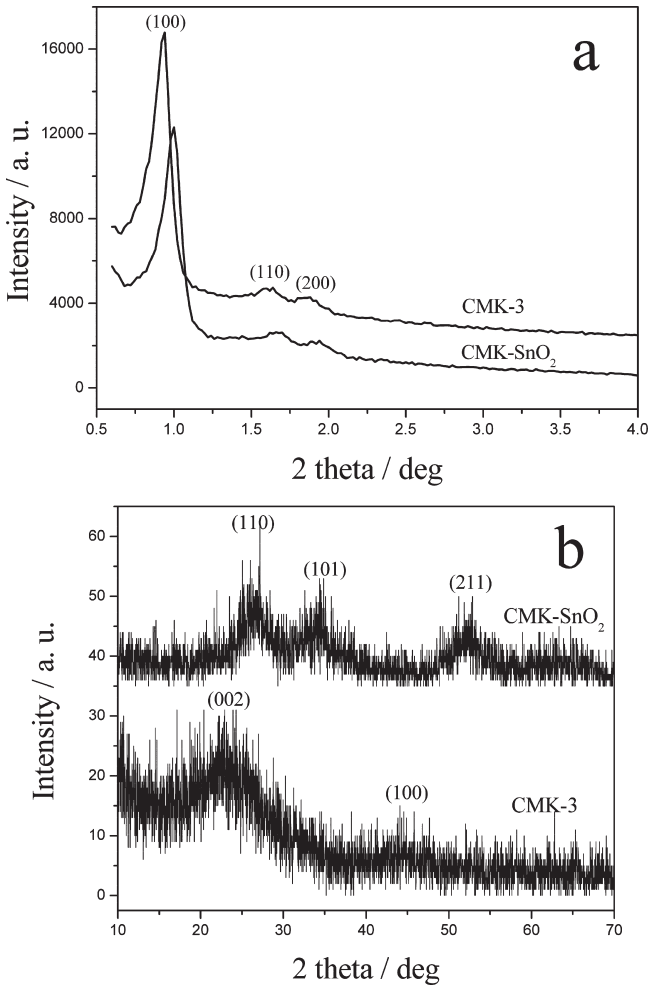

Figure 1. (a) Small-angle and (b) wide-angle XRD patterns of the CMK-3 and ordered SnO_2/CMK-3 nanocomposites samples.

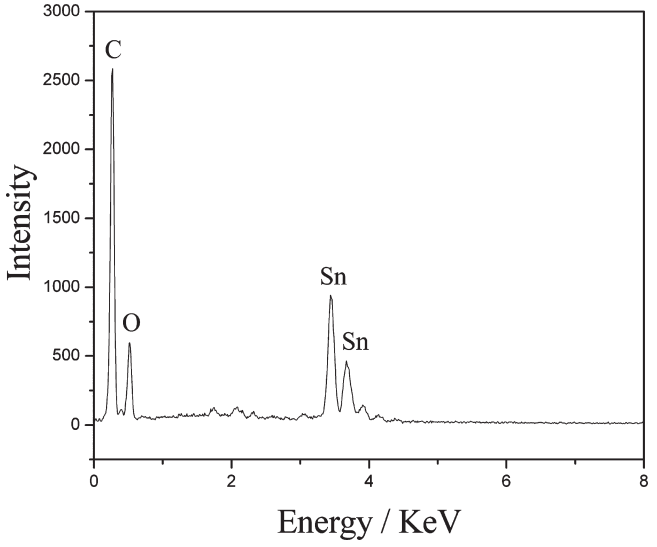

Figure 2. EDS spectrum of the ordered SnO_2/CMK-3 nanocomposites sample.

small-angle XRD. The two broad diffraction peaks of [002] and [100] of the graphite structure can also be observed in the

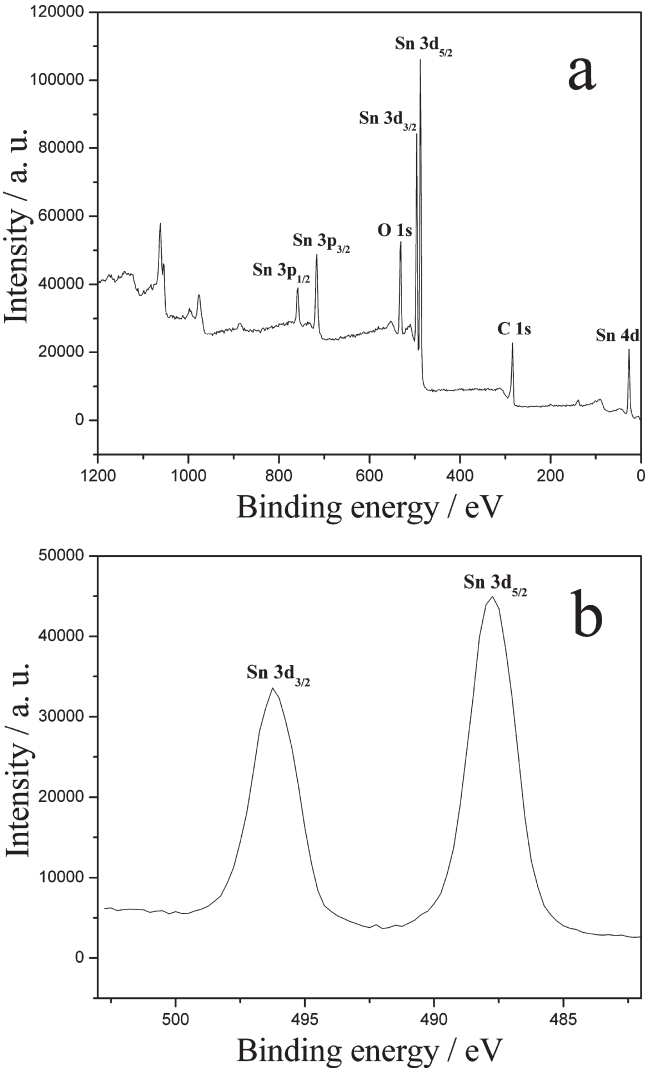

Figure 3. XPS spectra of (a) survey and (b) Sn 3d of the ordered SnO_2/CMK-3 nanocomposites sample.

wide-angle XRD pattern of CMK-3 shown in Figure 1b. These broad peaks indicated that CMK-3 includes very small amounts of stacked crystalline graphite phase. The wide-angle XRD pattern of ordered SnO_2/CMK-3 nanocomposites can be well indexed to the tetragonal structure of SnO_2 (JCPDS, No. 41−1445). Energy-dispersive spectroscopy (EDS) measurement results in Figure 2 revealed the presence of Sn, O, and C elements in the ordered SnO_2/CMK-3 nanocomposites sample, which shows the composition of SnO_2 in the composite. The EDS measurement illustrated that there was about 17 wt % of SnO_2 inside CMK-3.

X-ray photoelectron spectroscopy was used to investigate the surface chemical composition of ordered SnO_2/CMK-3 nanocomposites. XPS survey spectrum of ordered SnO_2/CMK-3 nanocomposites confirmed that the sample contained only Sn, O and C elements (Figure 3a). And binding energies for Sn $3d_{5/2}$, O 1s, and C 1s were 485.4, 531.0, and 284.6 eV, respectively. XPS signals of Sn 3d were observed at binding energies at around 487.8 (Sn $3d_{5/2}$) and 496.2 eV (Sn $3d_{3/2}$) (Figure 3b). Quantification of the XPS peak areas given that the surface ratio of Sn/O in the sample was about 0.54, which was very close to the

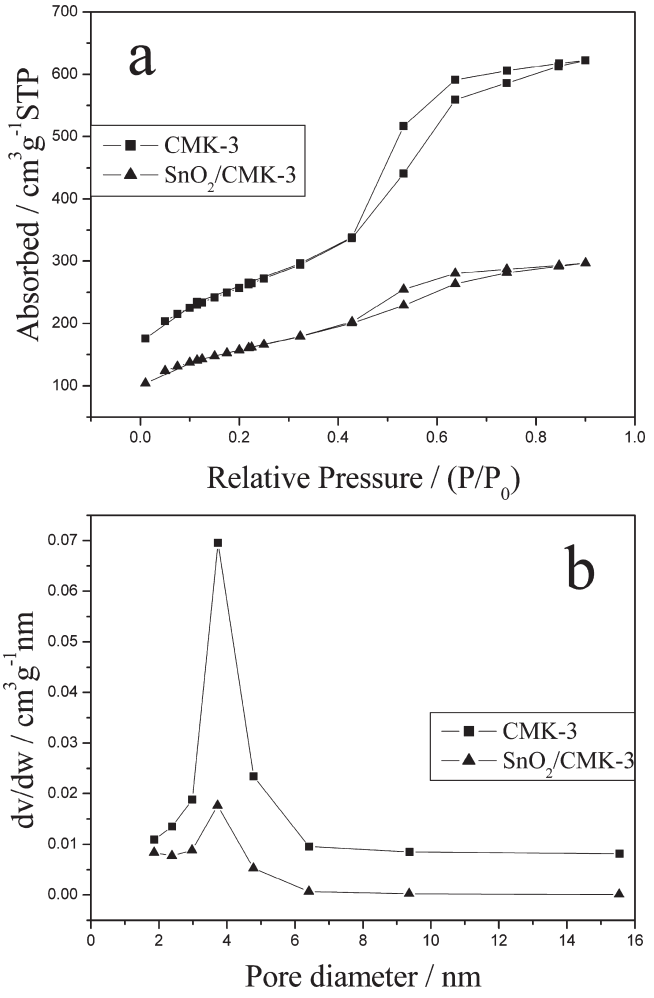

Figure 4. (a) Nitrogen adsorption−desorption isotherms, (b) pore size distribution curve of the CMK-3 and ordered SnO_2/CMK-3 nanocomposites samples.

Table 1. Surface Parameters of the CMK-3 and Ordered SnO_2/CMK-3 Nanocomposites Samples

sample	BET surface area ($m^2\ g^{-1}$)	BJH pore volume ($cm^3\ g^{-1}$)	pore size (nm)
CMK-3	956.7	1.09	3.9
SnO_2/CMK-3	648.8	0.54	3.4

chemical stoichiometry of Sn/O in the tin dioxides. Therefore, we concluded that the ordered SnO_2/CMK-3 nanocomposites consisted of SnO_2 and C on the basis of XRD, EDS, and XPS results.

A nitrogen isothermal adsorption technique was employed in order to investigate the ultrasonic irradiation effect on the pore structure as well as determining the location of SnO_2 in the CMK-3 host. Figure 4 shows the nitrogen adsorption−desorption isotherms and pore size distribution curves of the CMK-3 and ordered SnO_2/CMK-3 nanocomposites samples. The nitrogen adsorption−desorption isotherms shows that all samples were found to be of type IV isotherm curves with a marked leap in the adsorption at a relative pressure P/P_0 of 0.5 (Figure 4a), which was typical characteristics of mesoporous materials. The

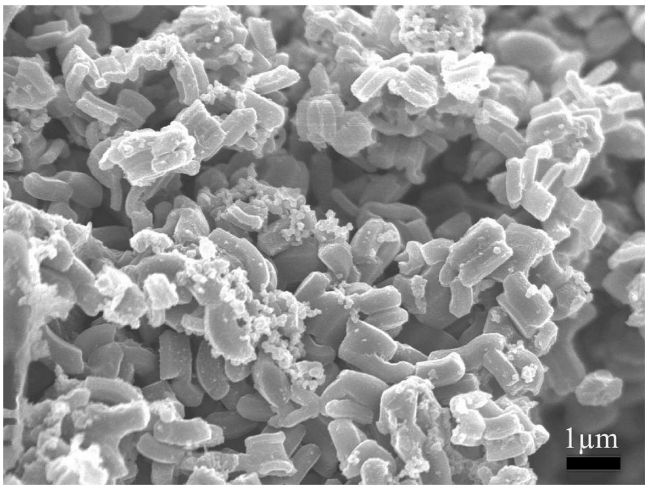

Figure 5. SEM image of the ordered SnO_2/CMK-3 nanocomposites sample.

Brunauer−Emmett−Teller (BET) specific surface area, pore volumes, and mean pore diameters of CMK-3 and ordered SnO_2/CMK-3 nanocomposites are summarized in Table 1. As indicated in Table 1, the surface area was found to decrease significantly from 956.7 $m^2\ g^{-1}$ for CMK-3 to 648.8 $m^2\ g^{-1}$ for ordered SnO_2/CMK-3 nanocomposites, and the average pore size was about 3.9 nm for CMK-3 and 3.4 nm for ordered SnO_2/CMK-3 nanocomposites (Figure 4b). Pore-filling would significantly reduce the surface area and pore size,[30,31] so we assumed that SnO_2 nanoparticles were formed inside the pore channels of CMK-3 for ordered SnO_2/CMK-3 nanocomposites.

Figure 5 shows SEM image of the ordered SnO_2/CMK-3 nanocomposites sample. From Figure 5, we can see that the SnO_2 nanoparticles were about 3 nm in diameter. TEM images were conducted to further confirm the existence of SnO_2 nanoparticles inside CMK-3. It is possible to discern directly the existence of SnO_2 nanoparticles in the channels of the CMK-3 for the ordered SnO_2/CMK-3 nanocomposites sample (Figure 6b) comparing with the original CMK-3 (Figure 6a). They were not very distinct, probably because of the weak contrast between the CMK-3 frameworks.[30] The uniform size of SnO_2 nanoparticles was about 3 nm, and no bulk aggregation of nanoparticles was observed on the outer surface. On the basis of the analysis above, we concluded that the SnO_2 nanoparticles were incorporated into CMK-3 pore channels.

Electrochemical performance demonstrated that the initial charge and discharge capacity of ordered SnO_2/CMK-3 nanocomposites electrode (CMK-3 with 17 wt % loading of SnO_2 nanoparticles) were 1913 and 690 mAh·g^{-1} at a C/10 charge/discharge rate (Figure 7a), respectively. The discharge capacity was much higher than that of CMK-3 electrode (449 mAh·g^{-1}). The irreversible capacity (1223 mA h g^{-1}) in the first cycle may be caused by the decomposition of the electrolyte on the surface of the active materials to form a passivation layer on the electrode (SEI film). Although there was obvious capacity loss in the initial few cycles, no significant capacity decay can be observed after five cycles. The specific capacity after 35 cycles for ordered SnO_2/CMK-3 nanocomposites electrode was 546 mA h g^{-1} (Figure 7b). This value was much higher than that of CMK-3 electrode (234 mA h g^{-1}). The ordered SnO_2/CMK-3 nanocomposites electrode also exhibited high capacity at higher charge/discharge

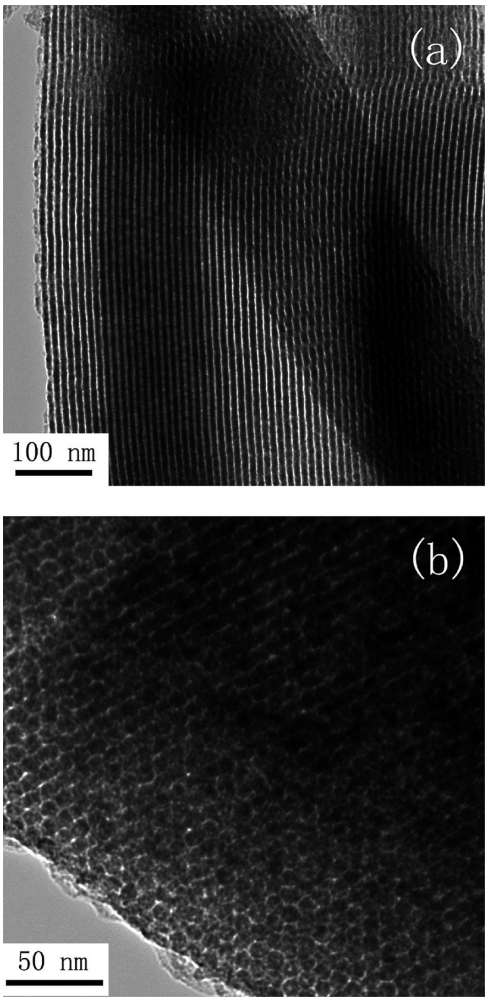

Figure 6. TEM images of the (a) CMK-3 and (b) ordered SnO_2/CMK-3 nanocomposites samples.

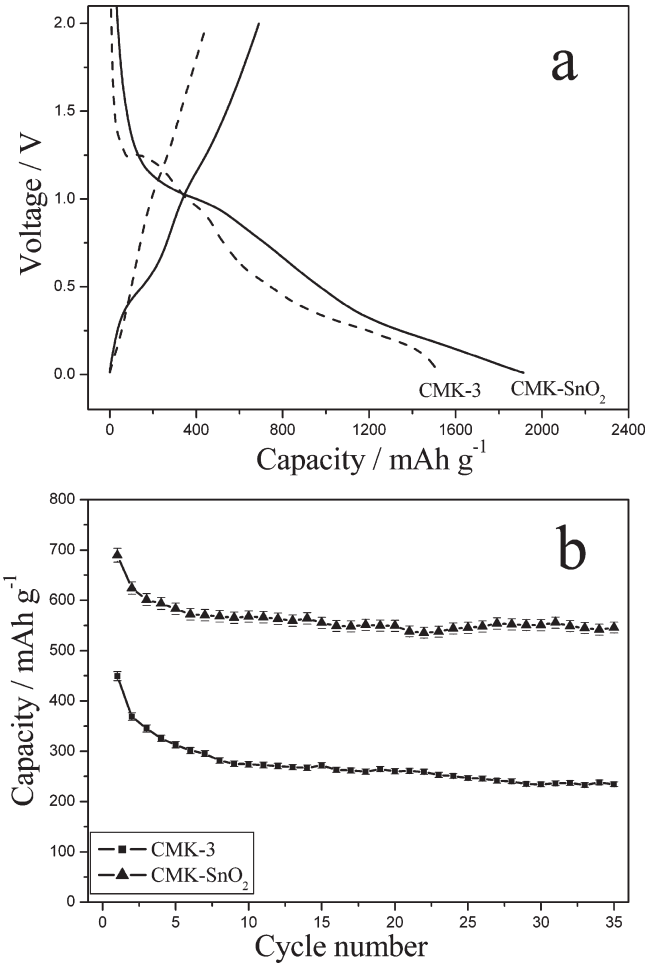

Figure 7. (a) Initial discharge−charge curves, (b) cyclic performance of the CMK-3 and ordered SnO_2/CMK-3 nanocomposites electrodes at a *C*/10 charge/discharge rate.

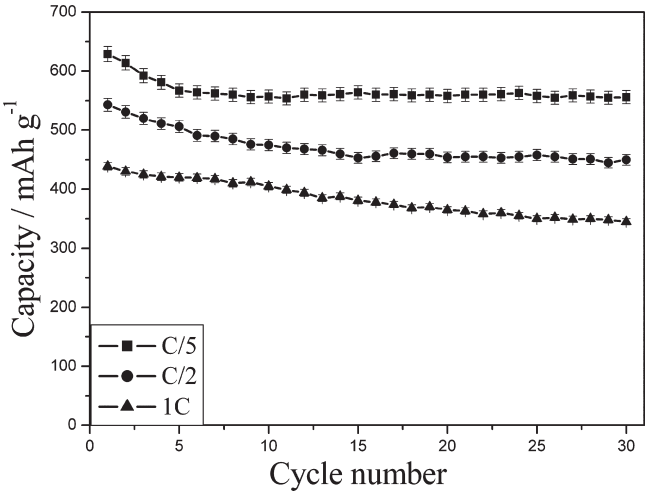

Figure 8. Rate capability of the ordered SnO_2/CMK-3 nanocomposites electrode.

rate. The discharge specific capacities of 629, 543, and 439 mA h g^{-1} are obtained at *C*/5, *C*/2, and 1*C* rates (Figure 8), respectively. There were several reasons for the improvement of electrochemical performance of ordered SnO_2/CMK-3 nanocomposites electrode. First, the electrode made of nanometer-sized SnO_2 formed inside CMK-3 ordered mesoporous carbon offered the possibility of combining good electronic conductivity of the carbon matrix and the high Li storage of SnO_2 into one incorporated entity. Second, the carbon framework hindered the aggregation of SnO_2 nanoparticles and provided enough space to buffer the volume changes during the lithium insertion and extraction reactions in SnO_2.[32,33] Finally, porous structures also have large surface areas, which permit high lithium-ion flux across the interface, reduce lithium-ion diffusion distance, and facilitate electron transfer to the current collector (copper foil) through the mesoporous structure.

In summary, we prepared SnO_2 nanoparticles inside the pore channels of ordered mesoporous carbon CMK-3 via sonochemical method. CMK-3 with 17 wt % loading of SnO_2 nanoparticles had a large specific surface area and pore volume. Electrochemical performance demonstrated that the ordered SnO_2/CMK-3 nanocomposites electrode possessed higher reversible capacity and cycling stability than that of original CMK-3 electrode. Moreover, the ordered SnO_2/CMK-3 nanocomposites electrode also exhibited high capacity at higher charge/discharge rate. The excellent electrochemical performances make the ordered SnO_2/CMK-3 nanocomposites a promising anode material for high-power

lithium-ion batteries. In the future, we will synthesize Sn nanoparticles inside the pore channels of ordered mesoporous carbon CMK-3 as a new promising anode material for high-power lithium-ion batteries.

EXPERIMENTAL SECTION

Synthesis. The synthesis process of ordered mesoporous carbon is similar to that described by Ryoo.[34] Before synthesizing SnO_2 nanoparticles inside CMK-3 by means of ultrasonic irradiation, surface modification of CMK-3 (hydrophilic) was performed in the following way: Ordered mesoporous carbon CMK-3 was treated with 1 M H_2SO_4 at 80 °C for 3 h, washed with distilled water, and dried at 80 °C. This sample was denoted as m-CMK-3. Further, 0.2 g of m-CMK-3 was dispersed into an aqueous solution of $SnCl_2 \cdot 2H_2O$ (0.02 M). After 3 h, the mixture was subjected to ultrasonic irradiation at room temperature. During irradiation, water flow was utilized to cool the glass vessel in the bath. After 2 h of irradiation, the precipitate was washed thoroughly with distilled water, and then dried at 120 °C for 12 h in a vacuum oven. The sample prepared was referred to ordered SnO_2/CMK-3 nanocomposites.

Characterization. X-ray diffraction patterns of the products were recorded on a X-ray diffractometer (MAC Science Co. Ltd. MXP 18 AHF) with monochromatized Cu Kα radiation (λ = 1.5406 Å). XPS measurements were performed in a VG Scientific ESCALAB Mark II spectrometer equipped with two ultrahighvacuum (UHV) chambers. Transmission electron microscopy (TEM) was performed on a transmission electron microscopy (Philip CM-120) at an accelerating voltage of 120 KV. The nitrogen adsorption and desorption isotherms were measured using Micrometrics ASAP2010 system.

Electrochemical Measurement. The working electrodes were prepared by mixing 80% ordered SnO_2/CMK-3 nanocomposites, 10% acetylene black, and 10% poly(tetrafluoroethylene) by weight with 2-propanol to form an paste. The paste was then roll-pressed into ca. 0.1 mm thick film and finally fixed onto a nickel net. The testing cells had a typical three-electrode construction using lithium foils as both counter electrodes and reference electrodes, and 1 M $LiPF_6$ dissolved in ethylene carbonate (EC), dimethyl carbonate (DMC) and ethylene methyl carbonate (EMC) (1:1:1, v/v/v) as the electrolyte. The cells were assembled in an argon-filled glovebox.

AUTHOR INFORMATION

Corresponding Author

*E-mail: qfwei@jiangnan.edu.cn (Q.W.); flh@jiangnan.edu.cn (F.H.). Tel/Fax: +86-510-8591 2009.

ACKNOWLEDGMENT

This work was financially supported by the Fundamental Research Funds for the Central Universities (JUSRP11102 and JUSRP20903), the National Natural Science Foundation of China (51006046), the Natural Science Fundation of Jiangsu Province (BK2010140), the Youth Science Foundation of Jiangnan University (2009LQN01), the Open Project Program of Key Laboratory of Eco-Textiles, Ministry of Education, Jiangnan University, China (KLET0908), and the Research Fund for the Doctoral Program of Higher Education of China (200802951011 and 20090093110004).

REFERENCES

(1) Eom, J. Y.; Kwon, H. S. *ACS Appl. Mater. Interfaces* **2011**, *3*, 1015–1021.
(2) Persson, K.; Sethuraman, V. A.; Hardwick, L. J.; Hinuma, Y.; Meng, Y. S.; Van der Ven, A.; Srinivasan, V.; Kostecki, R.; Ceder, G. *J. Phys. Chem. Lett.* **2010**, *1*, 1176–1180.
(3) Wu, P.; Du, N.; Zhang, H.; Zhai, C. S.; Yang, D. R. *ACS Appl. Mat. Interfaces* **2011**, *3*, 1946–1952.
(4) Camean, I.; Garcia, A. B. *J. Power Sources* **2011**, *196*, 4816–4820.
(5) Fujimoto, H.; Tokumitsu, K.; Mabuchi, A.; Chinnasamy, N.; Kasuh, T. *J. Power Sources* **2010**, *195*, 7452–7456.
(6) Li, Y. G.; Tan, B.; Wu, Y. Y. *Nano Lett.* **2008**, *8*, 265–270.
(7) Li, J. X.; Zhao, Y.; Guan, L. H. *Electrochem. Commun.* **2010**, *12*, 592–595.
(8) Zhou, H. S.; Zhu, S. M.; Hibino, M.; Honma, I.; Ichihara, M. *Adv. Mater.* **2003**, *15*, 2107–2111.
(9) Zhang, H. J.; Tao, H. H.; Jiang, Y.; Jiao, Z.; Wu, M. H.; Zhao, B. *J. Power Sources* **2010**, *195*, 2950–2955.
(10) Cheng, M. Y.; Hwang, B. J. *J. Power Sources* **2010**, *195*, 4977–4983.
(11) Nagao, M.; Otani, M.; Tomita, H.; Kanzaki, S.; Yamada, A.; Kanno, R. *J. Power Sources* **2011**, *196*, 4741–4746.
(12) Yin, X. M.; Chen, L. B.; Li, C. C.; Hao, Q. Y.; Liu, S. A.; Li, Q. H.; Zhang, E. D.; Wang, T. H. *Electrochim. Acta* **2011**, *56*, 2358–2363.
(13) Wu, F. D.; Wu, M. H.; Wang, Y. *Electrochem. Commun.* **2011**, *13*, 433–436.
(14) Li, L. M.; Yin, X. M.; Liu, S. A.; Wang, Y. G.; Chen, L. B.; Wang, T. H. *Electrochem. Commun.* **2010**, *12*, 1383–1386.
(15) Wang, C. M.; Xu, W.; Liu, J.; Zhang, J. G.; Saraf, L. V.; Arey, B. W.; Choi, D. W.; Yang, Z. G.; Xiao, J.; Thevuthasan, S.; Baer, D. R. *Nano Lett.* **2011**, *11*, 1874–1880.
(16) Li, J. X.; Zhao, Y.; Wang, N.; Guan, L. H. *Chem. Commun.* **2011**, *47*, 5238–5240.
(17) Cui, L. F.; Shen, J. A.; Cheng, F. Y.; Tao, Z. L.; Chen, J. *J. Power Sources* **2011**, *196*, 2195–2201.
(18) Lou, X. W.; Wang, Y.; Yuan, C.; Lee, J. Y.; Archer, L. A. *Adv. Mater.* **2006**, *18*, 2325–2329.
(19) Wang, Y.; Su, F. B.; Lee, J. Y.; Zhao, X. S. *Chem. Mater.* **2006**, *18*, 1347–1353.
(20) Luo, Q. P.; Lei, B. X.; Yu, X. Y.; Kuang, D. B.; Su, C. Y. *J. Mater. Chem.* **2011**, *21*, 8709–8714.
(21) Ataee-Esfahani, H.; Wang, L.; Nemoto, Y.; Yamauchi, Y. *Chem. Mater.* **2010**, *22*, 6310–6318.
(22) Mukherjee, S.; Das, D.; Chakrabarti, P. *J. Phys. Chem. C* **2010**, *114*, 14763–14771.
(23) Zhang, Y.; Hu, C. G.; Zheng, C. H.; Xi, Y.; Wan, B. Y. *J. Phys. Chem. C* **2010**, *114*, 14849–14853.
(24) Pinkas, J.; Reichlova, V.; Serafimidisova, A.; Moravec, Z.; Zboril, R.; Jancik, D.; Bezdicka, P. *J. Phys. Chem. C* **2010**, *114*, 13557–13564.
(25) Zhang, R. Z.; Dai, H. X.; Du, Y. C.; Zhang, L.; Deng, J. G.; Xia, Y. S.; Zhao, Z. X.; Meng, X.; Liu, Y. X. *Inorg. Chem.* **2011**, *50*, 2534–2544.
(26) Wei, X.; Xu, G.; Ren, Z. H.; Xu, C. X.; Weng, W. J.; Shen, G.; Han, G. R. *J. Am. Chem. Soc.* **2010**, *93*, 1297–1305.
(27) Hu, Z. A.; Xie, Y. L.; Wang, Y. X.; Mo, L. P.; Yang, Y. Y.; Zhang, Z. Y. *Mater. Chem. Phys.* **2009**, *114*, 990–995.
(28) Bhattacharyya, S.; Gabashvili, A.; Perkas, N.; Gedanken, A. *J. Phys. Chem. C* **2007**, *111*, 11161–11167.
(29) Seayad, A. M.; Antonelli, D. M. *Adv. Mater.* **2004**, *16*, 765–777.
(30) Zhang, W.; Shi, J.; Chen, H.; Hua, Z.; Yan, D. *Chem. Mater.* **2001**, *13*, 648–654.
(31) Li, L.; Shi, J. L.; Zhang, L. X.; Xiong, L. M.; Yan, J. N. *Adv. Mater.* **2004**, *16*, 1079–1082.
(32) Nara, H.; Fukuhara, Y.; Takai, A.; Komatsu, M.; Mukaibo, H.; Yamauchi, Y.; Momma, T.; Kuroda, K.; Osaka, T. *Chem. Lett.* **2008**, *37*, 142–143.
(33) Wang, D. H.; Kou, R.; Choi, D.; Yang, Z. G.; Nie, Z. M.; Li, J.; Saraf, L. V.; Hu, D. H.; Zhang, J. G.; Graff, G. L.; Liu, J.; Pope, M. A.; Aksay, I. A. *ACS Nano* **2010**, *4*, 1587–1595.
(34) Joo, S. H.; Choi, S. J.; Oh, I.; Kwak, J.; Liu, Z.; Terasaki, O.; Ryoo, R. *Nature* **2001**, *412*, 169–172.